AIP | Journal of Applied Physics

Analysis of the structure, configuration, and sizing of Cu and Cu oxide nanoparticles generated by fs laser ablation of solid target in liquids

J. M. J. Santillán, F. A. Videla, M. B. Fernández van Raap, D. C. Schinca, and L. B. Scaffardi

Citation: J. Appl. Phys. **113**, 134305 (2013); doi: 10.1063/1.4798387

View online: http://dx.doi.org/10.1063/1.4798387

View Table of Contents: http://jap.aip.org/resource/1/JAPIAU/v113/i13

Published by the American Institute of Physics.

Analysis of the structure, configuration, and sizing of Cu and Cu oxide nanoparticles generated by fs laser ablation of solid target in liquids

J. M. J. Santillán,[1] F. A. Videla,[1,2] M. B. Fernández van Raap,[3] D. C. Schinca,[1,2] and L. B. Scaffardi[1,2,a)]
[1]*Centro de Investigaciones Ópticas (CIOp), (CONICET La Plata - CIC), Argentina*
[2]*Departamento de Ciencias Básicas, Facultad de Ingeniería, UNLP, Argentina*
[3]*Departamento de Física-IFLP, Universidad Nacional de La Plata-CONICET, L. B. Scaffardi: CIOp CC3 (1897) Gonnet, La Plata, Argentina*

(Received 22 January 2013; accepted 13 March 2013; published online 2 April 2013)

We report on the analysis of structure, configuration, and sizing of Cu and Cu oxide nanoparticles (Nps) produced by femtosecond (fs) laser ablation of solid copper target in liquids. Laser pulse energy ranged between 500 μJ and 50 μJ. Water and acetone were used to produce the colloidal suspensions. The study was performed through optical extinction spectroscopy using Mie theory to fit the full experimental spectra, considering free and bound electrons size dependent contributions to the metal dielectric function. Raman spectroscopy and AFM technique were also used to characterize the sample. Considering the possible oxidation of copper during the fabrication process, two species (Cu and Cu_2O) arranged in two structures (bare core or core-shell) and in two configuration types (Cu-Cu_2O or Cu_2O-Cu) were considered for the fitting depending on the laser pulse energy and the surrounding media. For water at high energy, it can be observed that a Cu-Cu_2O configuration fits the experimental spectra of the colloidal suspension, while for decreasing energy and below a certain threshold, a Cu_2O-Cu configuration needs to be included for the optimum fit. Both species coexist for energies below 170 μJ for water. On the other hand, for acetone at high energy, optimum fit of the full spectrum suggests the presence a bimodal Cu-Cu_2O core-shell Nps distribution while for decreasing energy and below a 70 μJ threshold energy value, Cu_2O-Cu core-shell Nps must be included, together with the former configuration, for the fit of the full spectrum. We discuss possible reasons for the changes in the structural configuration of the core-shell Nps. © *2013 American Institute of Physics*. [http://dx.doi.org/10.1063/1.4798387]

I. INTRODUCTION

In the recent years, copper metal Nps and their oxides have been the subject of intense research due to their potential applications in broad areas of sciences and technology such as chemistry, catalysis, nanofluidics, material science, and high temperature superconductors.[1–5] Copper properties such as high conductivity, photosensitivity, and low cost makes it a promising material for chemical, electronic, and photonic integration in miniaturized devices for use in biological nanosensors,[6–10] as well as its capability of insertion in host polymer matrices for nonlinear optical applications.[11–13]

Optical properties such as extinction and plasmon resonance are highly size dependent below 10 nm. They also depend on host environment and particularly on the possible shell grown around the particle during the fabrication process that yields, in general, core-shell structure Nps. This fabrication processes may be based on wet chemistry methods or physical methods such as laser ablation of solid target in liquids or RF sputtering.

In all cases, it is necessary to determine the size and the structure of the Nps. In this sense, optical extinction spectroscopy has demonstrated its ability to size core radius and shell thickness of noble metal Nps through the fitting of the full UV-Vis extinction spectra using Mie's theory[14] together with a conveniently modified metal bulk complex dielectric function that includes the size correction of free and bound electrons contributions.[15–19]

During the last years, there has been a lot of research about Cu-Cu oxide nanocomposites[20–28] covering different aspects such as fabrication methods, optical properties, and structural analyses. From a general point of view, it can be said that knowledge of the mechanisms responsible for the formation of Cu-Cu oxide Nps is far from complete and may vary with the different conditions under which they were fabricated. Yin *et al.*[20] developed a copper (I) acetate high temperature thermal decomposition approach to form first Cu colloids that was gradually oxidized to form stable Cu_2O particles of about 6 nm size, as supported by XRD studies. However, some of their optical absorption results show a resonance at about 610 nm which was tentatively assigned by the authors to possible Cu core—Cu_2O shell Nps plasmon peak. Pike and co workers[21] applied time-resolved XRD to study a ramping temperature reduction experiment and showed that, while CuO reduces directly to Cu in bulk, at the nanoscale it follows a two-step pathway, reducing first to stable Cu_2O and then to Cu as temperature rises. From the results of their experiments, they suggest that there should be a critical particle size below which this sequential reduction takes place. Pedersen *et al.*[24] generated Cu Nps using magnetron DC sputtering of a high purity Cu target on a glass slide in an oxygen-free atmosphere. After exposing the obtained 3 nm diameter

a)e-mail: lucias@ciop.unlp.edu.ar

copper Nps to air at 160 °C, absorption spectra were taken at different times showing a reduction of the Cu plasmon peak and an enhancement of bands at lower wavelengths, consistent with the formation of Cu-Cu_2O core-shell Nps. Besides, oxidation of small Cu Nps yielded different oxide type depending on the range of temperatures in which the process occurs. A Cu Nps fabrication technique commonly used by many authors is pulsed laser ablation of solid target in liquids.[22,23,25,26] In these cases, the fundamental or second harmonic wavelength of a Q-switched 10 ns pulsed Nd:YAG laser was used. Tilaki *et al.*[22] produced with this method Cu Nps in water and acetone with sizes around 30 nm and 3 nm, respectively. Optical extinction spectra obtained at different times after fabrication show a Cu plasmon resonance around 600 nm, although somewhat different from the typical Cu resonance at 590 nm that can be obtained from Mie calculations. To explain this difference, the authors propose, among other reasons, oxidation of colloidal copper due to the reaction with dissolved oxygen in water, although no fitting of the experimental spectra was attempted. Amikura *et al.*[23] and Nath *et al.*[25] used the second harmonic of a 10 ns pulse Nd:YAG laser to ablate a copper target in water. The former produced cuprous oxide particles of varied sizes and morphology, observing in every case that the UV-visible spectra showed a peak at 650 nm, which the authors assigned to Cu-Cu oxide spherical Nps. The latter investigated the influence of focusing conditions (fluence) on the size and oxidation characteristics of the resulting colloids. Based on optical extinction spectroscopy as well as Raman spectroscopy of the colloids, they conclude that Cu core-Cu oxide shell Nps were fabricated. CuO type oxide of size less than 200 nm was formed in tightly focusing conditions, while Cu_2O type oxide, of size under 10 nm, appeared for defocusing conditions. Recently, Liu *et al.*[26] used the fundamental wavelength of a Nd:YAG laser to produce 30 nm diameter Cu_2O Nps from laser ablation of an electrolytic copper plate immersed in PVP. XRD and electron diffraction patterns showed that Cu particles draught-dried at room temperature oxidized completely to Cu_2O.

This work analyzes the structure, configuration, and size of different species of Nps obtained by ultrashort pulse laser ablation of solid copper target in different liquids based on UV-vis absorption spectroscopy, Raman spectroscopy, and Atomic Force Microscopy (AFM) images. We show that, besides the most cited Cu core-Cu oxide shell configuration, there appears a reverse conformation when low pulse energies are used. We discuss our results based on oxidation mechanisms of Nps during the fabrication process as studied by other authors.[20–28]

II. THEORETICAL BACKGROUND

In general, the complex dielectric function for bulk metals can be splitted into two terms, a free-electron term and an interband (or bound-electron term). Considering that the function is additive, it can be written as

$$\varepsilon_{size}(\omega,R) = \varepsilon_{bound-electrons}(\omega,R) + \varepsilon_{free-electrons}(\omega,R). \quad (1)$$

For bound electrons, the complex dielectric function arising due to transitions from the copper *d*-band to the conduction *s*-band, can be calculated using the expression given by Bigot *et al.*:[29]

$$\varepsilon_{bound-electrons}(\omega,R) = K_{size}(R)\int_{\omega_g}^{\infty}\frac{\sqrt{x-\omega_g}}{x}[1-F(x,T)] \times \frac{(x^2-\omega^2+{\gamma_b}^2+i\,2\,\omega\,\gamma_b)}{(x^2-\omega^2+{\gamma_b}^2)^2+4\,\omega^2{\gamma_b}^2}\,dx, \quad (2)$$

where $\hbar\omega_g$ is the gap energy (E_g) of copper, $F(x, T)$ is the Fermi energy distribution function of conduction electron of energy $\hbar\, x$ at the temperature T with Fermi energy E_F; γ_b represents the damping constant in the interband transition, and K_{size} is a radius dependent proportionality factor:[15] $K_{size}(R) = K_{bulk}\,(1-\exp\,(-R/R_0))$, R is the particle radius, R_0 is a scale factor, and K_{bulk} is the coefficient for bound electron contribution.

For free electrons, the complex dielectric function can be written as:

$$\varepsilon_{free-electrons}(\omega,R) = 1 - \frac{{\omega_p}^2}{\omega^2 + i\gamma_{size}\,(R)\,\omega}, \quad (3)$$

where ω_p is the bulk plasma frequency (13.4×10^{15} Hz).[30] γ_{size} (R) is the radius dependent damping constant in the Drude model:[31]

$$\gamma_{size}(R) = \gamma_{bulk} + C\frac{v_F}{R}, \quad (4)$$

with v_F being the electron velocity at the Fermi surface. Fermi velocity for copper was taken from[32] to be $v_F = 15.7\times10^{14}$ nm/s. C is a constant related to electron scattering processes within the particles whose value ranges between 0.5 and 1.2, as derived from first principles calculations.[33] In our case, a C value of 0.8 was used. The value of $\gamma_{bulk} = 1.45\times10^{14}$ Hz was taken from Johnson and Christy.[34]

When Eqs. (2)–(4) are introduced in Eq. (1) to fit the bulk dielectric function considering $R = 100$ nm ($R \gg R_0$), it is possible to determine the following parameters for copper: $K_{bulk} = 2\times10^{24}$, $E_g = 1.95$ eV, $E_F = 2.15$ eV, and $\gamma_b = 1.15\times10^{14}$ Hz.[35]

III. EXPERIMENTAL PROCEDURE

Colloidal Nps were fabricated by ultrafast pulse laser ablation in liquids. The target sample used to carry out these experiments was a 1 mm thick circular disk of high purity grade copper immersed in acetone or water. Laser ablation was performed using a Ti:Sapphire chirped pulsed amplification (CPA) system from Spectra Physics, emitting pulses of 100 fs width at 1 kHz repetition rate centered at 800 nm wavelength. The maximum output energy was 1 mJ per pulse, but it could be attenuated using a classical waveplate-polarizer system. A 5 cm focal length lens was used to focus the laser beam on the target disk surface. The pulse energies used in these experiments range from 500 μJ to 50 μJ. Considering the focal length of the focusing lens and the input beam diameter, the corresponding fluence values ranged from 450 J/cm^2 to

45 J/cm^2. The sample was moved using a XY motorized micrometric stage. The movement was programmed so that the laser impinged always in different points of the sample. In this way, ablation was performed always from a fresh surface of the sample. This process lasted 9 min, after which the large number of Nps generated in the suspension produced a typical greenish colour in water and reddish in acetone. Optical extinction spectroscopy was conducted by means of a Shimadzu spectrophotometer from 300 to 1000 nm. The sample preparation for this method precludes the development of agglomerates in spite of no ligand compounds were added to the solutions. Optical absorption measurements and Raman spectroscopy were performed on the obtained colloidal suspension 5 min after fabrication and further sonication. This direct and in situ measurement prevents possible coalescence of the Nps and provides reliable statistics. For the AFM images, part of the as-generated sample was diluted to a value of about 1:100 to ensure single particles observation. A drop of such diluted sample was placed on a freshly cleaved muscovite mica sheet (SPI Supplies) and dried for 40 min in an oven at 45 °C with mild nitrogen flux.

Images were recorded in air, at room temperature, and at a scan rate of 1 Hz, using standard semicontact mode AFM. NT-MDT Solver Pro equipped with a silicon cantilever (force constant 48 N/m, resonant frequency 500 kHz) holding a sharp tip of 10 nm curvature radius were used for scanning. Minimum scanning step in vertical direction was 0.012 nm.

IV. OPTICAL EXTINCTION CALCULATIONS

Since the size of the copper Nps considered in this paper is very small compared with the incident wavelength, the response to optical extinction can be described using the electrostatic approximation of Mie Theory. In this approach, the expression for the extinction cross section is

$$C_{ext.} = k' \ \mathrm{Im}\,(\alpha), \tag{5}$$

where α is the polarizability, $k' = \frac{2\pi n_m}{\lambda}$ is the wavenumber in the medium surrounding the particle, n_m is the refractive index of the medium, and λ is the wavelength of the incident light in vacuum. For the general case of spherical Nps with core-shell structure, the polarizability can be written as:[14]

$$\alpha = 4\pi R'^3 \frac{(\varepsilon_2 - \varepsilon_m)(\varepsilon_1 + 2\varepsilon_2) + f(\varepsilon_1 - \varepsilon_2)(\varepsilon_m + 2\varepsilon_2)}{(\varepsilon_2 + 2\varepsilon_m)(\varepsilon_1 + 2\varepsilon_2) + f(2\varepsilon_2 - 2\varepsilon_m)(\varepsilon_1 - \varepsilon_2)}, \tag{6}$$

where $f = (\frac{R}{R'})^3$ is the ratio between inner and outer radius volumes, $R = r_{core}$ is the radius of the central core, $R' = r_{(core+coating)}$ is the outer radius (core + shell thickness), $\varepsilon_1 = \varepsilon_1\ (\lambda,\ R)$, $\varepsilon_2 = \varepsilon_2\ (\lambda)$, and $\varepsilon_m = \varepsilon_m\ (\lambda)$ are the dielectric functions of the core, coating (shell) and surrounding medium, respectively. Another parameter related with the extinction cross section is the extinction coefficient defined as $Q_{ext} = C_{ext}/\pi R'^2$.

Taking into account that copper presents two types of oxidation states (Cu_2O and CuO) with different probability of synthesis according to a variety of experimental conditions such as temperature, fluence, and liquid media, it is interesting to give a brief overview on the generation of oxide-coated copper Nps fabricated by pulsed laser ablation as reported by other authors.[22,24,26,28] The mechanisms underlying the formation of copper Nps with pulsed laser ablation of a copper solid target in liquids are very complex. Oxidative processes of Cu Nps are complicated since copper has two oxidation states (Cu^{+1} and Cu^{+2}) that form stable oxides with different activation energy barriers. The extreme pressure and temperature conditions in the focal volume during laser ablation and their rapid variation in time makes the explanation about copper-oxide formation a difficult task. Tilaki *et al.*[22] mention the role of plasma plume-nanoparticle interaction in the growth mechanism of Nps by nucleation process, as well as oxidation of colloidal Cu due to the reaction with dissolved oxygen in water. Amikura *et al.*[23] support the concept also shared by Pedersen *et al.*[24] and Kabashin *et al.*[36] that the formation mechanism includes various reactions in nonequilibrium high-temperature high-pressure plasma-liquid environment and particles are formed in the cavitation bubbles generated in the laser breakdown. The Cu clusters formed after the adiabatic expansion (and cooling) of the plasma plume react with the solvent (oxhidrile radicals or oxygen atoms) to produce copper oxides. Liu *et al.*[26] demonstrated the production of only Cu_2O Nps from laser ablation of electrolytic copper plates immersed in PVP. Nath and Khare[25] described the formation of copper oxide Nps in a nanosecond regime high power pulsed laser ablation for different focussing conditions. The shockwave that results from the laser breakdown generates high pressure-high temperature conditions at the liquid-plasma interface, which becomes an active chemical reaction zone that enhances the bonding of copper species with ionized water molecules to form copper oxide Nps. The extreme pressure and temperature conditions encountered at the solid target-liquid interface dominate the size and structural phase of the synthesized Nps. Their results from Raman spectra indicate that for nanosecond low fluence regime, Cu_2O Nps are more probable than CuO Nps. They also conclude from UV-visible absorption spectra that Cu-Cu_2O core-shell structures are also formed during the ablation process. Taking into account these reports about the appearance of cuprous oxide as well as previous work by the authors on Ag-Ag_2O Nps,[18] it is pertinent to analyze the characteristics of optical extinction spectra of small spherical assuming a possible core-shell Cu-Cu_2O Nps structure.

Considering Eq. (6) it is possible to calculate the extinction cross section for subnanometric and nanometric copper particles with and without Cu_2O shell. Figure 1(a) shows the spectrum for a bare core (zero shell thickness) subnanometric Cu particle of 0.7 nm radius together with that corresponding to the same Cu Np capped with 0.35 nm thickness of Cu_2O (50% of core radius). Both spectra are normalized to their plasmon peak value for comparison purposes. It can be seen that there is a considerable redshift of the peak position for the Cu-Cu_2O structure (about 70 nm for the considered sizes) and an increase of the slope for wavelengths below 600 nm in the extinction spectrum when an oxide shell thickness is considered. The inset shows the complex dielectric function of the Cu_2O used in the calculations, according to the data given by Ref. 34.

Figure 1(b) shows similar behaviour for copper Nps of 4 and 10 nm radius, with a Cu_2O shell thickness of 0% R (bare core) and 50% R (core-shell). In this case, the shell also produces a noticeable redshift, together with a sharper definition of the peak. Besides, the short wavelength tail of the capped Nps is very different in shape compared with the bare core Nps.

V. RESULTS AND DISCUSSION

Based on peak position and full spectrum shape behaviours with core size and shell thickness shown in Figure 1, it was possible to characterize the experimental copper Nps extinction spectra fabricated by ultrashort pulse laser ablation of solid target in different liquid media and different pulse energies. All experimental spectra were taken 5 min after fabrication and plotted normalized to unity at plasmon resonance peak for comparison purposes. The general characteristics of our spectra (peak position and tails at short and at long wavelengths) are very similar to those obtained by Tilaki *et al.*,[22] although these authors never attempted a full spectrum fit.

Figures 2(a) and 2(b) show the experimental extinction spectra obtained at different fs pulse energy between 500 μJ and 50 μJ in water and acetone, respectively.

It is interesting to notice that these normalized spectra have different shapes as the laser pulse energy goes from high values to low values and the plasmon peak wavelength is redshifted for low energies. The difference in shape is more evident for the case of water (Fig. 2(a)), particularly in the short wavelength tail from 300 nm to 500 nm. The inset shows separately the spectra corresponding to 100 μJ and 200 μJ, where it can be seen not only the difference in short wavelengths tail slope but also a slight redshift of the plasmon peak. Based on our previous study of the size dependent Cu dielectric function,[35] we now set for reproducing the experimental extinction spectra using core and shell size as fitting parameters. This assumption of a core-shell structure is based on the observation of this kind of structure using HRTEM imaging obtained in a previous work.[35]

Figure 3(a) shows the experimental extinction spectrum corresponding to colloidal suspension Nps in water fabricated with 500 μJ pulse energy (red full line) together with the theoretical fit (full diamond and dashed line). The

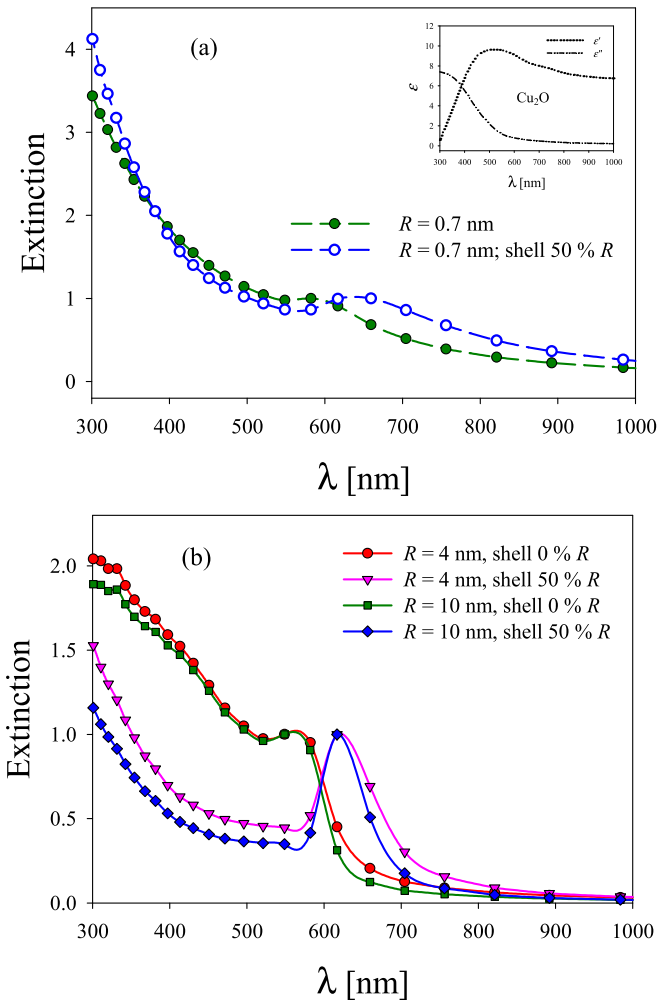

FIG. 1. Theoretical optical extinction spectra of copper bare core Nps compared with a core-shell Cu-Cu_2O Nps with the same core and 50% of shell thickness: (a) subnanometric and (b) nanometric. The shell produces a measurable redshift of the plasmon peak. Inset in panel (a) shows the dielectric function of Cu_2O taken from Palik.

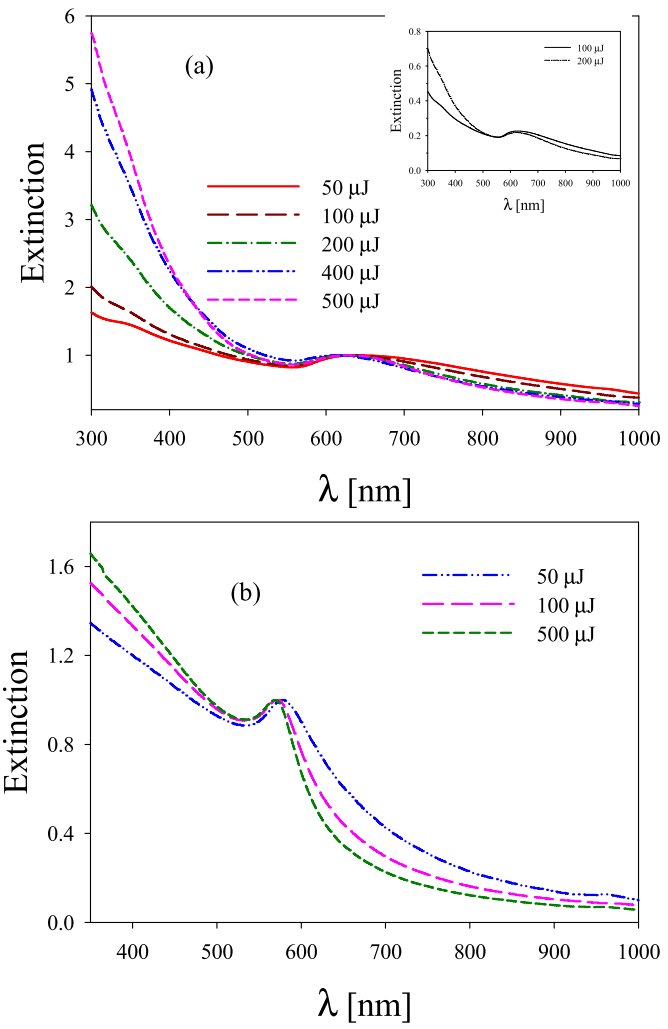

FIG. 2. Experimental extinction spectra of copper Nps fabricated by fs pulse laser ablation at different pulse energies in different surrounding media: (a) in water and (b) in acetone

latter was calculated using Eqs. (5) and (6) for the extinction cross section and polarizability and Eqs. (1)–(4) for the dielectric functions of the copper core and Cu_2O shell. It can be seen that the broad peak at 650 nm (Cu plasmon) is reproduced as well as the short and long wavelength tails of the full spectrum.

This optimum fit is attained only for a colloidal suspension containing Cu-Cu_2O subnanometric particles, mainly of 0.9 nm core radius, with two distinct oxide thicknesses of 40% and 150% of core radius (distribution histogram inset in Figure 3(a)). This narrow distribution may be interpreted in terms of the particular characteristics of the fabrication process at these high energies in which the particles are fabricated and sequentially fragmented by linear absorption.

To shed light on the type of copper oxide formed in the ultrashort pulse laser ablation process it is important to check the ability to fit this experimental spectrum using CuO instead of Cu_2O as the shell material. Figure 3(b) shows this comparison for the same core size and shell thickness values as in Figure 3(a). The inset shows the behaviour of the real and imaginary part of CuO dielectric function with wavelength.

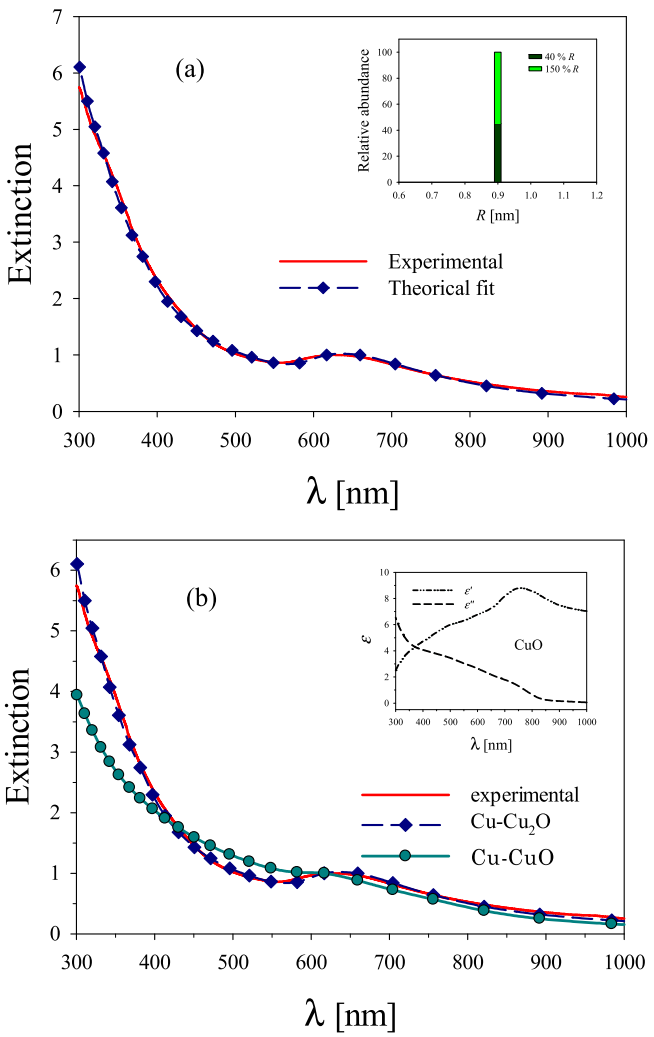

FIG. 3. (a) Experimental spectrum of colloidal suspensions fabricated in water with 500 μJ pulse energy and a theoretical fit considering a core-shell structure of the Cu-Cu_2O type. (b) Comparison between the fits of the same experimental spectrum using Cu-Cu_2O and Cu-CuO core-shell structures.

Notice the different shape of these curves with respect to the curves for Cu_2O shown in the inset of Figure 1(a). It can be seen that there is a noticeable disagreement between the experimental spectrum (full red line) and the fit using Cu-CuO core-shell configuration (full circles-full line): the plasmon peak is barely noticeable, its wavelength is blue shifted and the derivative of the spectrum in the short wavelength range is smaller than in the experimental spectrum. Furthermore, no combination of core size and shell thickness using this metal-metal oxide distribution was found to reproduce the spectrum. The theoretical fit using Cu-Cu_2O configuration (full diamond–dashed line) is included for agreement comparison.

An independent check of the presence of the Cu_2O as the shell material for the theoretical calculation, in accordance with conclusions stated by other authors,[25,26] a Raman spectrum using a 532 nm incident wavelength was obtained for the same colloidal sample fabricated with 500 μJ pulse energy (Figure 4).

The peaks indicated by full diamonds correspond to resonant transitions of 108 cm^{-1} (Γ_{12}), 165 cm^{-1} ($\Gamma_{12}^{(1)}$), and 232 cm^{-1} (2 $\Gamma_{12}^{(-)}$) of Cu_2O.[37,38] The peak appearing at 50 cm^{-1} is a tail of the strong Rayleigh line, while the feature starting at about 550 cm^{-1} is the onset of the water Raman band, extending up to about 3000 cm^{-1}. The known prominent CuO Raman peak at 297 cm^{-1} was not observed, indicating the absence of this kind of oxide.

During our ablation experiments in water and acetone, it was observed that for a sequential laser pulse energy decrease, the short wavelength tail of the spectra decreases its slope while the contrast $\left(\frac{I_{peak}-I_{valley}}{I_{peak}}\right)$ increases slightly. Figure 5 shows the extinction spectrum of copper colloidal suspension in water for 100 μJ pulse energy. It can be observed that the experimental spectrum presents the characteristic UV peaks in the range 300–360 nm, corresponding to Brillouin transitions of Cu_2O, in agreement with the spectra shown by Nath and Khare.[25]

For this case of low energy, it was not possible to find a set of parameters that could fit the full spectrum considering only the Cu-Cu_2O configuration used for water at high

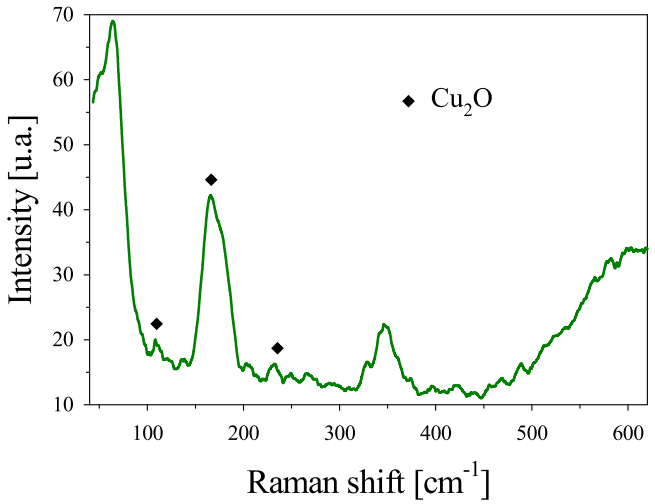

FIG. 4. Raman spectrum corresponding to copper in water with E = 500 μJ pulse energy. Peaks correspond to resonant transitions of Γ_{12} (108 cm^{-1}), $\Gamma_{12}^{(1)}$ (165 cm^{-1}) and 2 $\Gamma_{12}^{(-)}$ (232 cm^{-1}) of Cu_2O.

energy. As shown in the inset of Figure 5, the best fit was obtained including two types of structures: one of them corresponds to Cu_2O-Cu Nps with a dominant (60%) 3 nm core radius and different shell thicknesses, 30% of 2 nm core radius and a small abundance (less than 5%) of 5 nm core radius. The other structure corresponds to bare Cu_2O Nps of 10 nm radius. The change in conformation of the core-shell structure and the broadening of the size distribution is noticeable when the laser pulse energy decreases. From the fitting of the experimental spectra for different laser pulse energy, there seems to be an energy threshold at about 150 μJ for water below which the Cu_2O-Cu configuration dominates. Our results about the formation of Cu_2O core Nps by fs laser ablation of a copper plate in aqueous solution agree in general with those obtained by Liu *et al.*,[26] who worked with ns-pulses laser ablation.

A possible explanation can be formulated recalling the results obtained by Pike *et al.*,[21] where copper oxide particles reduce to Cu as temperature increases. The temperature at which this phase transition occurs is size dependent. For small particles (less than 10 nm), a Cu_2O-Cu configuration is formed for temperatures in the range 400 to 500 °C. For higher temperatures (over 500 °C), this structure reduces to metallic Cu. Since during fs laser ablation these temperatures are easily reached in the plasma plume[39] and in the plasma-liquid interface[25] during a time interval compatible with the fast oxidation kinetics at the nanoscale (about 100 ns), it is possible to argue that, under our experimental conditions, Nps with the Cu_2O-Cu configuration are generated in the colloidal suspension.

The formation of a metallic copper shell around the bare Cu_2O Nps can be explained based on the results of Amoruso *et al.*[40] and Grojo *et al.*[41] about the generation of metallic Nps in solution. After a fs laser pulse impinges on the sample, high pressure and high temperature plasma is produced on the solid-liquid interface. The adiabatic expansion that follows this event leads to rapid cooling of the plasma plume and hence to cluster formation. Nps are formed after a time delay

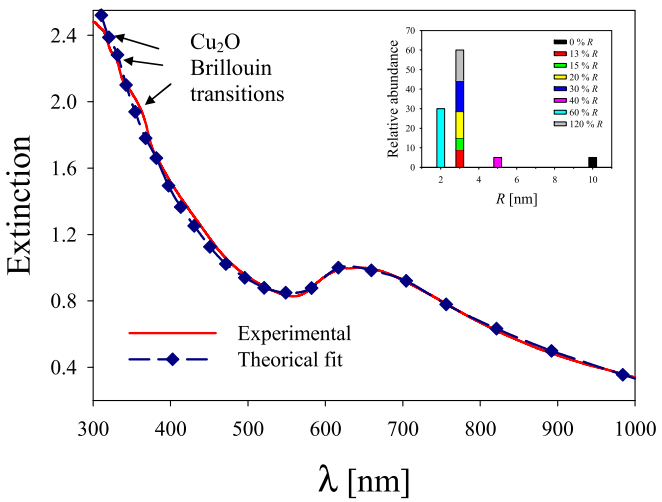

FIG. 5. Experimental spectra of colloidal suspensions fabricated in water with 100 μJ pulse energy. Theoretical fit was obtained with Cu_2O-Cu and Cu_2O Nps. The inset shows the optimal size distribution of core radii and shell thickness that best fits the experimental spectrum.

of about 5 to 30 μs,[39] time by which the temperature has fallen below 1000 K approximately.[40] With the extinguishment of the plasma, the formed Nps may interact with the oxygen generated in the solvent by the laser pulse, starting an oxidation reaction that leads to the Cu_2O component of the core-shell Nps. This oxidation may be complete or incomplete, mainly according to the local oxygen atom concentration. If oxidation is complete, the formed Cu_2O Nps may be reached by the following laser pulse, which will increase its temperature and produce a reducing reaction[21] that leads to the formation of a metallic Cu-shell around the bare Cu_2O Nps.

To compare our sizing results with a direct observation, an AFM and HRTEM studies of the 100 μJ colloid sample was carried out. Figure 6 shows these results. Panel (a) shows an AFM image of a 40 μm by 40 μm area, where spherical shape nanoparticles can be seen, thus supporting the use of Mie approach for calculating the polarizability and the extinction spectra. It can also be seen that dilution was enough to allow single particle observation. Panel (b) shows representative height profiles of the six lines scanned in panel (a). Individual particle size is accurately retrieved. The registered heights (diameters of the particles) are in agreement with the external radii distribution determined from the fit of the extinction spectrum of the sample (considering a core-shell structure). For these small size values, it is important to consider the roughness of the mica substrate on which the drop was deposited. Panel (c) depicts the AFM image of a free mica area and panel (d) its height profile. It can be seen that the mean roughness is more than one order of magnitude smaller than the smallest recorded particle, so there is a very good signal-to-noise ratio in the nanoparticle's profile. Panel (e) shows the HRTEM image of the same colloidal suspension. It can be seen that the Nps are spherical in shape and with a size distribution in agreement, both with the AFM results and with the distribution retrieved from extinction spectroscopy.

When acetone was used instead of water as suspension medium, similar results were obtained. Figure 7 shows the experimental curves (red full line) and the theoretical fit (full diamond and dashed line) corresponding to copper Nps in acetone fabricated with (a) 500 μJ, (b) 100 μJ, and (c) 50 μJ pulse energy, respectively. Fitting of the experimental curves was performed using Eq. (6), considering different spherical structures with two types of core-shell configurations with a distribution of size and shell thickness. The inset in each panel shows the relative abundance of different core radii with shell thickness distribution for each radius that yield optimum fit of full spectrum. It must be stressed here that the distribution histograms that fit the experimental spectra are the result of an iterative process that changes sequentially different parameters such as core radii, shell thickness, and core-shell configuration. Each parameter modifies an independent feature of the spectra (plasmon peak, plasmon width and slope at long and short wavelengths), so the optimum set is unique in the sense that there is no other set of parameters that fit correctly the full spectrum.

In the case of Figure 7(a), the optimum fit suggests the presence of a bimodal Cu-Cu_2O core-shell Nps, with a core size distribution (inset histogram) composed by small core radii in the range 0.8 to 4 nm and a larger one centered at

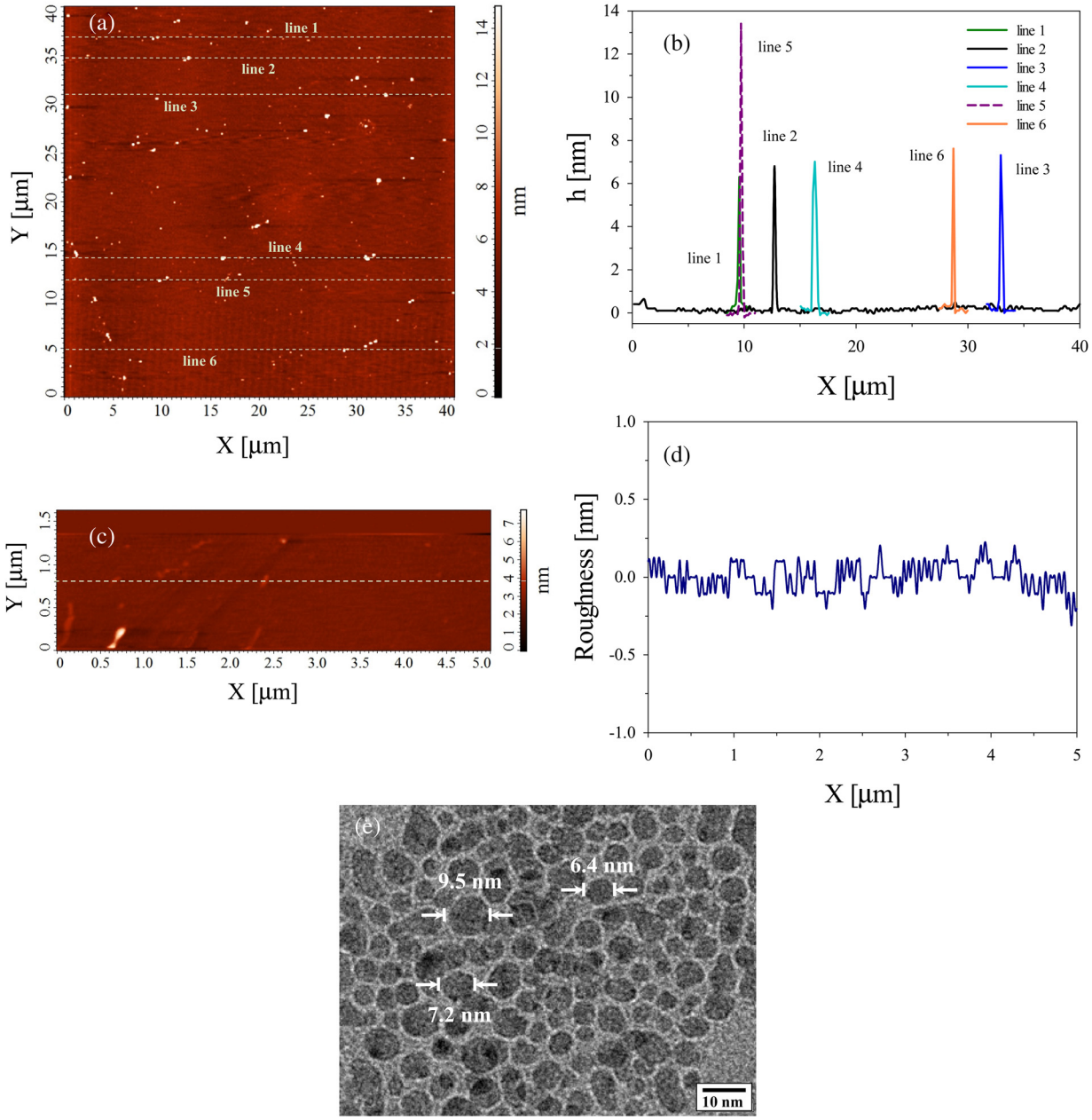

FIG. 6. (a) AFM image of copper Nps in water obtained with 100 μJ pulse energy, (b) height profiles of the six horizontal lines shown in panel (a), (c) AFM image of free area of the mica substrate used in the image, (d) height profile of image in panel (c), (e) HRTEM image of the same colloidal suspension.

10 nm. The subnanometric contribution has an abundance of 32%, while the 2 nm Cu bare core Nps has a dominant (47%) abundance. The inset histogram also shows the shell thickness distribution, suggesting also a bimodal distribution of small thicknesses (less than 5% core radius) and large thicknesses (about 150% core radius).

Fit of the spectrum in Figure 7(b) shows also a bimodal distribution with small and large core radii of Cu-Cu_2O Nps. The former has a 68% abundance of 1 nm core radius particle with 0.25 nm shell thickness and 24% abundance of 0.6 nm core radius particles with 0.3 nm shell thickness, while the latter has a small percentage contribution of 10 nm core radius particle with 0.5 nm shell thickness. Although this latter abundance is small compared with the former ones, it is important to include it since large particles have larger extinction spectra than smaller ones and approach better the long wavelength tail of the experimental spectrum. Comparison of the histograms in Figures 7(a) and 7(b) suggests that the oxide shell thickness decreases as the laser pulse energy decreases.

The experimental spectrum for 50 μJ energy is shown in Figure 7(c) and deserves special attention. The corresponding theoretical fit could only be obtained considering two core-shell type configurations: an 81% of Cu-Cu_2O Nps with 4 nm core radius and the remaining 19% corresponding to Cu_2O-Cu with different core radius and moderates shell thickness. Inclusion of the latter configuration allows obtaining a suitable fit of the long wavelength tail. It must be pointed out that it was impossible to fit the whole spectrum only considering the Cu-Cu_2O core-shell configuration. From the results of our experiments in acetone with different

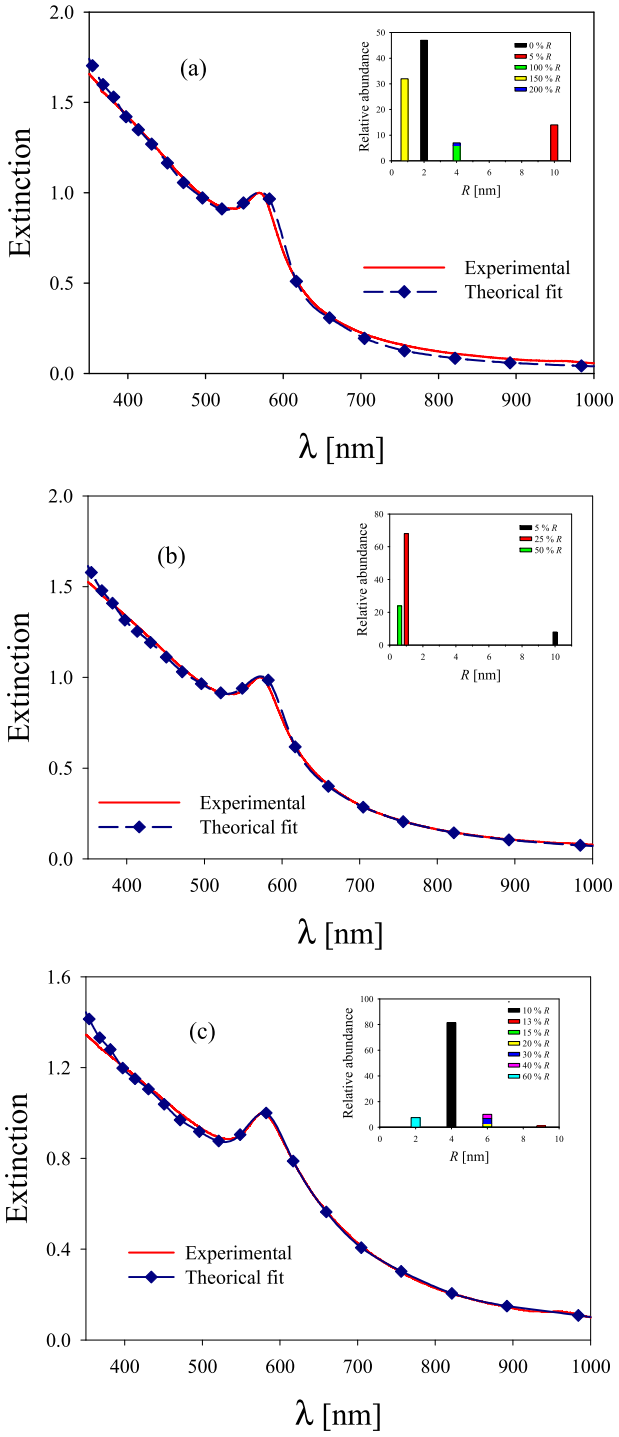

FIG. 7. Experimental spectra and theoretical fit of colloidal suspension in acetone: (a) pulse energy E = 500 μJ, (b) pulse energy E = 100 μJ, and (c) pulse energy E = 50 μJ. In each panel, the inset shows the optimal size distribution of core radii and shell thickness that fits the whole experimental spectrum. The fit in panel (a) is based on a combination of Cu bare core and Cu-Cu_2O structures. The fit in panel (b) is based on Cu-Cu_2O structure, while the fit in panel (c) is based on a combination of Cu-Cu_2O and Cu_2O-Cu configurations.

pulse energies, a threshold value of about 70 μJ was determined below which the Cu_2O-Cu starts to appear.

Summarizing our results obtained in water and acetone, it may be said that there is a threshold pulse laser energy below which both kind of configurations coexist, whose relative abundance depends on the liquid medium.

VI. CONCLUSIONS

We have analyzed the structure, configuration and sizing of Cu and Cu oxide Nps generated by fs laser ablation of copper solid target in water and acetone using different laser pulse energies between 500 μJ and 50 μJ. Several techniques were used such as extinction spectroscopy, Raman spectroscopy, and AFM. The extinction spectra of the obtained colloidal suspensions show the typical copper Np plasmon resonance in the 580 nm to 650 nm range. The obtained Nps are spherical and small in size (less than 10 nm radius), thus enabling the fit of the extinction spectra using the electrostatic approximation of Mie theory. For the correct fit of the peak position and full spectrum, it was necessary to consider the fact that copper Nps were oxidized in the fabrication process, generating core-shell type structures of different configurations (Cu-Cu_2O and Cu_2O-Cu) depending on laser pulse energy. The type of copper oxide appearing around the Nps was determined by Raman spectroscopy. The size, structural formation, and configuration of these Nps could be determined by fitting the extinction spectra.

For water, high pulse energies yield almost monodispersed subnanometric Cu-Cu_2O Nps but, as the energy decreases, there seems to be a threshold value at about 150 μJ, below which a reverse configuration (Cu_2O-Cu) starts to appear, coexisting with the former. This possibility is also supported by results in oxide reduction studies of copper Nps made by several authors.

For the case of acetone, a bimodal core-shell size distribution is generated for high and moderate energies, while for low energies (below 70 μJ), there is a trend to form Cu_2O-Cu with a non negligible abundance and thickness distribution that also coexists with Cu-Cu_2O.

The colloidal suspension samples were independently studied through AFM and HRTEM analysis. The size distributions derived from these two methods show very good agreement with the size derived from extinction spectra analysis.

Summarizing, the results of this work show that in the generation of core-shell Cu Nps by fs laser ablation, there exists a threshold energy (which depends on the type of the liquid medium) above which the Cu-Cu_2O configuration dominates and below which the reverse configuration start to appear and coexists with the former. Since optical extinction spectroscopy is very sensitive to small changes in core size and shell thickness, it allowed a very accurate fitting of the spectra. This fact makes it a reliable and complementing method to other used techniques such as high resolution TEM (HRTEM), AFM, and Raman spectroscopy among others.

ACKNOWLEDGMENTS

This work was performed by grants PIP (CONICET) 0394, PME 2006-00018 (ANPCyT), 11/I151 (Facultad de Ingeniería, Universidad Nacional de La Plata) and funds from IFLP-CONICET, Argentina. Daniel C. Schinca and Fabián A. Videla are members of CIC, Comisión de Investigaciones Científicas de la Provincia de Buenos Aires. L. B. Scaffardi and M. B. Fernández van Raap are researchers of CONICET,

and Jesica M. J. Santillán is fellow of CONICET, Argentina. TEM measurements were performed by Diego Muraca (Instituto de Física "Gleb Wataghin"- IFGW, Universidade Estadual de Campinas, Brazil) whose help is deeply acknowledged. Authors thank FAPESP and C2NANO—Center for Nanocience and Nanotechnology/ TEM-MSC-14827 for the use of TEM equipment.

[1]H. Zhu, C. Zhang, and Y. Yin, "Novel synthesis of copper nanoparticles: influence of the synthesis conditions on the particle size," Nanotechnology **16**, 3079 (2005).
[2]H. Wang, Y. Huang, Z. Tan, and X. Hu, "Fabrication and characterization of copper nanoparticle thin-films and the electrocatalytic behavior," Anal. Chim. Acta **526**, 13–17 (2004).
[3]G. Larsen and S. Noriega, "Dendrimer-mediated formation of Cu–CuO_x nanoparticles on silica and their physical and catalytic characterization," Appl. Catal., A **278**, 73–81 (2004).
[4]M. K. Patel, B. J. Nagare, D. M. Bayul, S. K. Haram, and D. C. Kothari, "Controlled synthesis of Cu nanoparticles in fused silica and BK7 glasses using ion beam induced defects," Surf. Coat. Technol. **196**, 96–99 (2005).
[5]J. M. Zuo, M. Kim, M. O'Keefe, and J. C. H. Spence, "Direct observation of *d*-orbital holes and Cu–Cu bonding in Cu_2O," Nature (London) **401**, 49–52 (1999).
[6]J. A. Dieringer, A. D. McFarland, N. C. Shah, D. A. Stuart, A. V. Whitney, C. R. Yonson, M. A. Young, X. Zhang, and R. P. Van Duyne, "Introductory lecture surface enhanced Raman spectroscopy: new materials, concepts, characterization tools, and applications," Faraday Discuss. **132**, 9–26 (2006).
[7]J. Zhao, A. Das, X. Zhang, G. C. Schatz, S. G. Sligar, and R. P. Van Duyne, "Resonance surface plasmon spectroscopy: low molecular weight substrate binding to cytochrome P450," J. Am. Chem. Soc. **128**, 11004–11005 (2006).
[8]A. M. Moran, J. Sung, E. M. Hicks, R. P. Van Duyne, and G. K. Spears, "Second harmonic excitation spectroscopy of silver nanoparticle arrays," J. Phys. Chem. B **109**, 4501–4506 (2005).
[9]A. J. Haes, W. P. Hall, L. Chang, W. L. Klein, and R. P. Van Duyne, "A localized surface plasmon resonance biosensor: first steps toward an assay for Alzheimer's disease," Nano Lett. **4**, 1029–1034 (2004).
[10]J. Jiang, K. Bosnick, M. Maillard, and L. Brus, "Single molecule Raman spectroscopy at the junctions of large Ag nanocrystals," J. Phys. Chem. B **107**, 9964–9972 (2003).
[11]A. Quaranta, R. Ceccato, C. Menato, L. Pederiva, N. Capra, and R. Dal Maschio, "Formation of copper nanocrystals in alkali-lime silica glass by means of different reducing agents," J. Non-Cryst. Solids **345–346**, 671–675 (2004).
[12]T. N. Rostovshchikov, V. V. Smirnov, V. M. Kozhevin, D. A. Yavsin, M. A. Zabelin, I. N. Yassievich, and S. A. Gurevich, "New size effect in the catalysis by interacting copper nanoparticles," Appl. Catal., A **296**, 70–79 (2005).
[13]Y. Gotoh, R. Igarashi, Y. Ohkoshi, M. Nagura, K. Akamatsu, and S. Deki, "Preparation and structure of copper nanoparticle/poly(acrylicacid) composite films," J. Mater. Chem. **10**, 2548–2552 (2000).
[14]C. F. Bohren and D. R. Huffman, *Absorption and Scattering of Light by Small Particles* (Wiley, New York, 1998).
[15]L. B. Scaffardi and J. O. Tocho, "Size dependence of refractive index of gold nanoparticles," Nanotechnology **17**, 1309–1315 (2006).
[16]M. V. Roldán, L. B. Scaffardi, O. de Sanctis, and N. Pellegri, "Optical properties and extinction spectroscopy to characterize the synthesis of amine capped silver nanoparticles," Mater. Chem. Phys. **112**, 984–990 (2008).
[17]D. C. Schinca and L. B. Scaffardi, "Core and shell sizing of small silver coated nanospheres by optical extinction spectroscopy," Nanotechnology **19**, 495712-8 (2008).
[18]D. C. Schinca, L. B. Scaffardi, F. A. Videla, G. A. Torchia, P. Moreno, and L. Roso, "Silver-silver oxide core-shell nanoparticles by femtosecond laser ablation: core and shell sizing by extinction spectroscopy," J. Phys. D: Appl. Phys. **42**, 215102-9 (2009).
[19]J. M. J. Santillán, L. B. Scaffardi, and D. C. Schinca, "Quantitative optical extinction-based parametric method for sizing a single core–shell Ag–Ag_2O nanoparticle," J. Phys. D: Appl. Phys. **44**, 105104-8 (2011).
[20]M. Yin, C.-K. Wu, Y. Lou, C. Burda, J. T. Koberstein, Y. Zhu, and S. O6ĈBrien, "Copper oxide nanocrystals," J. Am. Chem. Soc. **127**, 9506–9511 (2005).
[21]J. Pike, S.-W. Chan, F. Zhang, X. Wang, and J. Hanson, "Formation of stable Cu_2O from reduction of CuO nanoparticles," Appl. Catal., A **303**, 273–277 (2006).
[22]R. M. Tilaki, A. Iraji Zad, and S. M. Mahdavi, "Size, composition and optical properties of copper nanoparticles prepared by laser ablation in liquids," Appl. Phys. A **88**, 415–419 (2007).
[23]K. Amikura, T. Kimura, M. Hamada, N. Yokoyama, J. Miyazaki, and Y. Yamada, "Copper oxide particles produced by laser ablation in water," Appl. Surf. Sci. **254**, 6976–6982 (2008).
[24]D. B. Pedersen, S. Wang, and S. H. Liang, "Charge-transfer-driven diffusion processes in Cu@Cu-oxide core-shell nanoparticles: oxidation of 3.0 ± 0.3 nm diameter copper nanoparticles," J. Phys. Chem. C **112**, 8819–8826 (2008).
[25]A. Nath and A. Khare, "Size induced structural modifications in copper oxide nanoparticles synthesized via laser ablation in liquids," J. Appl. Phys. **110**, 043111 (2011).
[26]P. Liu, Z. Li, W. Cai, M. Fang, and X. D. Luo, "Fabrication of cuprous oxide nanoparticles by laser ablation in PVP aqueous solution," RSC Adv. **1**, 847–851 (2011).
[27]K. Mitsuo, "Laser-induced fragmentative decomposition of fine CuO powder in acetone as highly productive pathway to Cu and Cu_2O nanoparticles," J. Phys. Chem. C **115**, 5165–5173 (2011).
[28]T. Ghodselahi and M. A. Vesaghi, "Localized surface plasmon resonance of Cu@Cu_2O core-shell nanoparticles: absorption, scattering and luminescence," Physica B **406**, 2678–2683 (2011).
[29]J. Y. Bigot, V. Halté J. C. Merle, and A. Daunois, "Electron dynamics in metallic nanoparticles," Chem. Phys. **251**, 181–203 (2000).
[30]W. Cai and V. Shalaev, *Optical Metamaterials. Fundamentals and Applications* (Springer, Berlin, 2010).
[31]C. G. Granqvist and O. Hunderi, "Optical properties of ultrafine gold particles," Phys. Rev. B **16**, 3513–3534 (1977).
[32]G. W. C. Kaye and T. H. Laby, *Tables of Physical and Chemical Constants and Some Mathematical Functions* (Longman Scientific and Technical, London, 1995).
[33]U. Kreibig and M. Vollmer, *Optical Properties of Metal Clusters* (Springer, Berlin, 1995).
[34]P. B. Johnson and R. W. Christy, "Optical constants of the noble metals," Phys. Rev. B **6**, 4370–4379 (1972).
[35]J. M. J. Santillán, F. A. Videla, M. B. Fernández van Raap, D. C. Schinca, and L. B. Scaffardi, "Size dependent Cu dielectric function for plasmon spectroscopy. Characterization of colloidal suspension generated by fs laser ablation," J. Appl. Phys. **112**, 054319-1–054319-8 (2012).
[36]A. V. Kabashin and M. Meunier, *Laser Ablation Based Synthesis of Nanomaterials in Recent Advances in Laser Processing of Materials*, edited by J. Perriere, E. Million, and E. Fogarassy (Elsevier, 2006).
[37]D. Powell, A. Compaan, J. R. Macdonald, and R. A. Forman, "Raman-scattering study of ion-implantation-produced damage in Cu_2O," Phys. Rev. B **12**, 20–25 (1975).
[38]M. Balkanski, A. Nusimovici, and J. Reydellet, "First order Raman spectrum of Cu_2O," Solid State Commun. **7**, 815–818 (1969).
[39]J. König, S. Nolte, and A. Tünnermann, "Plasma evolution during metal ablation with ultrashort laser pulses," Opt. Express **13**, 10597–10607 (2005).
[40]S. Amoruso, G. Ausanio, R. Bruzzese, M. Vitiello, and X. Wang, "Femtosecond laser pulse irradiation of solid targets as a general route to nanoparticle formation in a vacuum," Phys. Rev. B **71**, 033406-4 (2005).
[41]D. Grojo, J. Hermann, and A. Perrone, "Plasmon analyses during femtosecond laser ablation of Ti, Zr, and Hf," J. Appl. Phys. **97**, 063306-9 (2005).